Delft University of Technology

Document Version
Final published version

Licence
CC BY

Citation (APA)
van Manen, D. J., Aichele, J., Müller, J., Serra-Garcia, M., & Wapenaar, K. (2026). Acoustic, electromagnetic, and elastic space-time media that compute their own inverse. *Physical Review Research*, *8*(3), Article 033358. https://doi.org/10.1103/hghj-fgsw

Important note
To cite this publication, please use the final published version (if applicable).
Please check the document version above.

Copyright
In case the licence states “Dutch Copyright Act (Article 25fa)”, this publication was made available Green Open Access via the TU Delft Institutional Repository pursuant to Dutch Copyright Act (Article 25fa, the Taverne amendment). This provision does not affect copyright ownership.
Unless copyright is transferred by contract or statute, it remains with the copyright holder.

Sharing and reuse
Other than for strictly personal use, it is not permitted to download, forward or distribute the text or part of it, without the consent of the author(s) and/or copyright holder(s), unless the work is under an open content license such as Creative Commons.

Takedown policy
Please contact us and provide details if you believe this document breaches copyrights.
We will remove access to the work immediately and investigate your claim.

This work is downloaded from Delft University of Technology.

Acoustic, electromagnetic, and elastic space-time media that compute their own inverse

Dirk-Jan van Manen,* Johannes Aichele, and Jonas Müller
Department of Earth and Planetary Sciences, ETH Zurich, Sonneggstrasse 5, 8092 Zurich, Switzerland

Marc Serra-Garcia
AMOLF, Science Park 104, 1098 XG Amsterdam, The Netherlands

Kees Wapenaar
Department of Geoscience and Engineering, TU Delft, Stevinweg 1, 2628 CN Delft, The Netherlands

(Received 12 December 2023; accepted 25 August 2026; published 23 September 2026)

Time materials are materials with acoustic, electromagnetic, or elastic properties that change while waves are propagating through them. Waves can scatter from such temporal inhomogeneities, but due to causality, they cannot reflect back in time. As a result, time-scattered wave fields do not resemble space-scattered wave fields—which are spatially mirrored—but instead look like copies of the original signal traveling back in time. Consequently, they can form an ingredient for physical solvers of inverse problems that rely on time-reversal transformations. Here, we investigate the use of time reflections for calculating so-called focusing wave fields. We establish a one-to-one mapping between focusing wave fields and the transmitted wave fields produced by time scattering. This mapping is then used to construct a space-time medium where the time scattering anticipates the space scattering and "computes" the exact inverse transmission response for the space scattering. We demonstrate the construction with a simple numerical example of a single pulse encountering a series of time boundaries before reaching a spatial inhomogeneity. The time boundaries scatter the single pulse into a focusing wave field that subsequently focuses through the spatial inhomogeneity. With certain mild assumptions, the transmitted wave has both the same wave shape and amplitude as the original pulse, yielding a transmission coefficient of unity.

DOI: 10.1103/hghj-fgsw

I. INTRODUCTION

Physical computing aims to find solutions to hard numerical problems by harnessing physical phenomena that directly evaluate the desired function [1–4]. Physical computers range from image generators that optically sample a diffusion model [5] to metamaterials that evaluate integrals and derivatives [6,7] and even perform voice [8,9] and image recognition [10,11]. A particularly challenging computational task is to solve *inverse problems*—identifying the inputs or parameters of a system that result in a specific output response. Many inverse methods hinge on the construction of a time-mirrored evolution of the system dynamics, which allows the propagation of sensitivities from the final state to the initial configuration. For example, the adjoint method in seismic imaging computes gradients by injecting the data residuals at receiver locations and propagating them backward in time through (essentially) the same wave operator, so the error wave field refocuses onto the causative structures [12,13]. Analogously in machine learning, backpropagation through time computes sensitivities by sending error signals backward through a recurrent neural network [14–16], and Hamiltonian echo backpropagation exploits time reversibility to run an "echo" that carries an injected error perturbation backward through a physical Hamiltonian system to obtain parameter updates [17–20]. These examples illustrate the importance of computing time-reversed wave fields for solving inverse problems. In this article, we will explore the physical computation of focusing functions—input wave fields that compensate internal reflections and thus produce a clean pulse inside the material—using time media, materials whose properties change over the timescales associated with wave propagation.

Scattering at time boundaries [21,22] offers intriguing new possibilities for wave control. It has recently been exploited to achieve *volumetric* time reversal [23]: Since all waves in a wave front scatter back energy when "encountering" a time boundary, those backscattered waves exactly retrace the path to the source, no matter how complex the original wave front was. Furthermore, it has been noticed that there is a similarity between time scattering and reverse-space scattering: Salem and Caloz [24] discuss a space-time cross-mapping method to show how time scattering can be used to facilitate the computation of solutions to certain space-scattering problems. Employing the cross-mapping method, one first computes the

*Contact author: vdirk@ethz.ch

Published by the American Physical Society under the terms of the Creative Commons Attribution 4.0 International license. Further distribution of this work must maintain attribution to the author(s) and the published article's title, journal citation, and DOI.

TABLE I. Quantities in the unified equations (after Ref. [30]).

	U	V	P	Q	α	β	a	b
1. AC waves	$-\Theta$	m_x	p	v_x	κ	ρ	q	f_x
2. TE waves	D_y	B_z	E_y	H_z	ϵ	μ	$-J_y^e$	$-J_z^m$
3. TM waves	B_y	$-D_z$	H_y	$-E_z$	μ	ϵ	$-J_y^m$	J_z^e
4. SH waves	m_y	$-2e_{yx}$	v_y	$-\tau_{yx}$	ρ	μ^{-1}	f_y	$2h_{yx}$

inverse of the cross-mapped problem nonrecursively using time scattering. The solution to the original problem can then be obtained by inverting the time-scattering solution and inverse cross-mapping it. Here, we go one step further and show how a time medium can be combined with a space medium, to yield a space-time medium that computes its own inverse. Thus, a single pulse entering the space-time medium on one side yields a single pulse on the other side and under certain conditions the transmission coefficient of the medium is unity. The reflection coefficient is nonzero, however.

This article is organized as follows. First, we present the basic equations governing space and time scattering in one-dimensional (1D) acoustic, electromagnetic, and elastic media in a unified notation. Then, we derive transmission and reflection coefficients for a space boundary, followed by the corresponding coefficients for a time boundary. Then, we compare the derived time transmission and reflection coefficients to transmission and reflection coefficients derived for so-called reverse-space scattering and show that they are equal up to a scaling. Reverse-space scattering coefficients appear in seismology [25,26] in the construction of focusing wave fields that are inverses for space scattering. This allows us to establish a mapping between focusing wave fields and the transmitted wave field produced by time scattering. We then show how a particular space-time medium can be constructed where the time scattering anticipates the space scattering and "computes" the exact inverse for the space scattering. The construction is illustrated with a simple numerical example.

Finally, while the current work concerns itself with space-time scattering in media governed by 1D scalar wave equations, theoretical developments in time scattering are neither limited to 1D nor limited to scalar wave equations (see, e.g., Refs. [27–29]).

II. THEORY

We present the theory in the unified notation of Wapenaar *et al.* [30], which governs wave propagation in 1D acoustic, electromagnetic, and elastic space-time media. The basic equations in the unified notation are

$$\partial_t U + \partial_x Q = a, \tag{1a}$$

$$\partial_t V + \partial_x P = b, \tag{1b}$$

where $U(x,t)$, $V(x,t)$, $P(x,t)$, and $Q(x,t)$ are space- and time-dependent wave-field quantities and $a(x,t)$ and $b(x,t)$ are space- and time-dependent source quantities (see Table I). Partial derivatives with respect to space and time are denoted by ∂_x and ∂_t, respectively. The constitutive equations relate the wave-field quantities:

$$U = \alpha P, \tag{2a}$$

$$V = \beta Q, \tag{2b}$$

where $\alpha(x,t)$ and $\beta(x,t)$ are the parameters of space- and time-dependent materials. Rows 2 and 3 contain the quantities for electromagnetic wave propagation, with TE standing for transverse electric and TM for transverse magnetic. Row 4 governs the propagation elastic waves, with SH standing for horizontally polarized shear. In this work, we show examples for row 1, which is concerned with acoustic wave propagation, denoted by AC. The relevant quantities and their units are dilatation $\Theta(x,t)$ (unitless), longitudinal mechanical momentum density $m_x(x,t)$ (in $\mathrm{kg\,m^{-2}\,s^{-1}}$), acoustic pressure $p(x,t)$ (in Pa), longitudinal particle velocity $v_x(x,t)$ (in $\mathrm{m\,s^{-1}}$), compressibility $\kappa(x,t)$ (in $\mathrm{Pa^{-1}}$), mass density $\rho(x,t)$ (in $\mathrm{kg\,m^{-3}}$), volume-injection rate density $q(x,t)$ (in $\mathrm{s^{-1}}$), and external longitudinal force density $f_x(x,t)$ (in $\mathrm{N\,m^{-3}}$). Note that the units provided here are for a quasi-1D system. For a detailed description of the quantities in the other rows, please refer to Ref. [30].

A. Space transmission and reflection coefficients

Although the derivation of transmission and reflection coefficients for a space boundary can be found in many textbooks, we repeat it here so that it can be effectively contrasted with the subsequent derivation for a time boundary.

We first consider a time-independent inhomogeneous material with parameters $\alpha(x)$ and $\beta(x)$. Substituting the constitutive equations (2) into Eq. (1), we find

$$\alpha\partial_t P + \partial_x Q = a, \tag{3a}$$

$$\beta\partial_t Q + \partial_x P = b. \tag{3b}$$

For a space-dependent material with piecewise continuous parameters, these equations are supplemented with boundary conditions at all points, where $\alpha(x)$ and $\beta(x)$ undergo a finite jump. The boundary conditions are that $P(x,t)$ and $Q(x,t)$ are continuous at these points.

Taking $x = 0$ as the location where the material properties change, the fields on either side of the space boundary can be written as

$$P_1(x = 0^-, t) = P_2(x = 0^+, t), \tag{4a}$$

$$Q_1(x = 0^-, t) = Q_2(x = 0^+, t), \tag{4b}$$

where 0^- and 0^+ denote the limit of x approaching zero from left and right sides, respectively. We define the AC/TE impedances (SH/TM admittances) in the space media:

$$\eta_1 = \sqrt{\frac{\beta_1}{\alpha_1}} \quad (x < 0), \tag{5a}$$

$$\eta_2 = \sqrt{\frac{\beta_2}{\alpha_2}} \quad (x > 0). \tag{5b}$$

Left of the space boundary, we consider incident and reflected waves with amplitudes A_I^x and A_R^x, propagating

in the positive and negative x direction with velocity $c_1 = (\alpha_1\beta_1)^{-1/2}$:

$$\left.\begin{aligned} P_1 &= A_I^x\delta((x/c_1)-t) + A_R^x\delta((x/c_1)+t) \\ Q_1 &= \eta_1^{-1}\big[A_I^x\delta((x/c_1)-t) - A_R^x\delta((x/c_1)+t)\big] \end{aligned}\right\}, \quad x<0. \tag{6}$$

Right of the space boundary, we consider a transmitted wave with amplitude A_T^x, propagating in the positive x direction with velocity $c_2 = (\alpha_2\beta_2)^{-1/2}$:

$$\left.\begin{aligned} P_2 &= A_T^x\delta((x/c_2)-t) \\ Q_2 &= \eta_2^{-1}A_T^x\delta((x/c_2)-t) \end{aligned}\right\}, \quad x>0. \tag{7}$$

Using the continuity conditions (4) in combination with Eqs. (6) and (7), we obtain

$$\big[A_I^x + A_R^x\big] = A_T^x, \tag{8a}$$

$$\eta_1^{-1}\big[A_I^x - A_R^x\big] = \eta_2^{-1}A_T^x. \tag{8b}$$

Defining the space transmission and reflection coefficients, $T^x = A_T^x/A_I^x$ and $R^x = A_R^x/A_I^x$, respectively, we find

$$T_{12}^x = \left(\frac{2\eta_2}{\eta_2+\eta_1}\right), \tag{9a}$$

$$R_{12}^x = \left(\frac{\eta_2-\eta_1}{\eta_2+\eta_1}\right), \tag{9b}$$

where the first digit in the subscript of the coefficients denotes the incident medium.

Wave-number shift for waves scattering at a space boundary

The boundary conditions (4) dictate that the *temporal* waveform is preserved for waves scattering at a space boundary. This implies that waves scattering at a space boundary undergo a wave-number shift. This shift is implicitly included in the delta functions, which can be seen by taking the *temporal* Fourier transform of, e.g., $\delta((x/c)-t)$:

$$\int_{-\infty}^{\infty}\delta((x/c)-t)\,e^{i\omega t}\,dt = e^{i\omega(x/c)} = e^{ikx},$$

with $k=\omega/c$. For the different velocities, $k_1=\omega/c_1$, whereas $k_2=\omega/c_2$. Hence, $k_2=(c_1/c_2)k_1$. Hence, if the propagation velocity changes across the boundary, the scattered waves will experience a wave-number shift proportional to the ratio of the propagation velocities.

B. Time transmission and reflection coefficients

Next, we consider a time-dependent homogeneous material with parameters $\alpha(t)$ and $\beta(t)$. Substituting the constitutive equations (2) into Eq. (1), we find

$$\partial_t U + \beta^{-1}\partial_x V = a, \tag{10a}$$

$$\partial_t V + \alpha^{-1}\partial_x U = b. \tag{10b}$$

For a time-dependent material with piecewise continuous parameters, these equations must be supplemented with boundary conditions at all time instants, where $\alpha(t)$ and $\beta(t)$ undergo a finite jump. The current scientific consensus is that U and V are continuous at a time boundary (see, e.g., Ref. [31] and references therein). Therefore, taking $t=0$ as the moment where the material properties change, the fields on either side of the time boundary can be written as

$$U_1(x,t=0^-) = U_2(x,t=0^+), \tag{11a}$$

$$V_1(x,t=0^-) = V_2(x,t=0^+), \tag{11b}$$

where 0^- and 0^+ denote the limit of t approaching zero from negative and positive times, respectively. The impedances (admittances) on either side of the time boundary are as in Eq. (5) (with t replacing x in the inequalities).

To facilitate comparison with reverse-space transmission and reflection coefficients derived later, we formulate the incident, transmitted, and reflected waves in terms of P and Q.

Before the time boundary, we consider a wave with amplitude A_I^t propagating in the positive x direction with propagation velocity $c_1 = (\alpha_1\beta_1)^{-1/2}$:

$$\left.\begin{aligned} P_1 &= A_I^t\delta(x-c_1t) \\ Q_1 &= \eta_1^{-1}A_I^t\delta(x-c_1t) \end{aligned}\right\}, \quad t<0. \tag{12}$$

Note that there is no reflected wave in material 1, since causality prevents waves from reflecting into the past. After the time boundary, we consider waves with amplitudes A_T^t and A_R^t propagating in the positive and negative x directions, respectively, with propagation velocity $c_2 = (\alpha_2\beta_2)^{-1/2}$:

$$\left.\begin{aligned} P_2 &= A_T^t\delta(x-c_2t) + A_R^t\delta(x+c_2t) \\ Q_2 &= \eta_2^{-1}\big[A_T^t\delta(x-c_2t) - A_R^t\delta(x+c_2t)\big] \end{aligned}\right\}, \quad t>0. \tag{13}$$

Using the continuity conditions (11) and the constitutive equations (2) in combination with Eqs. (12) and (13), we obtain

$$\alpha_1 A_I^t = \alpha_2\big[A_T^t + A_R^t\big], \tag{14a}$$

$$\beta_1\eta_1^{-1}A_I^t = \beta_2\eta_2^{-1}\big[A_T^t - A_R^t\big]. \tag{14b}$$

Defining the time transmission and reflection coefficients, $T^t = A_T^t/A_I^t$ and $R^t = A_R^t/A_I^t$, we find

$$T_{12}^t = \frac{1}{2}\left(\frac{\alpha_1}{\alpha_2} + \frac{c_2}{c_1}\right) = \left(\frac{c_2}{c_1}\right)\left(\frac{\eta_2+\eta_1}{2\eta_1}\right), \tag{15a}$$

$$R_{12}^t = \frac{1}{2}\left(\frac{\alpha_1}{\alpha_2} - \frac{c_2}{c_1}\right) = \left(\frac{c_2}{c_1}\right)\left(\frac{\eta_2-\eta_1}{2\eta_1}\right), \tag{15b}$$

where the first digit in the subscript of the coefficients denotes the incident medium.

Frequency shift for waves scattering at a time boundary

Note that the boundary conditions (11) dictate that the *spatial* waveform is preserved for waves scattering at a time boundary. This implies that waves scattering at a time boundary undergo a frequency shift. This shift is implicitly included in the delta functions, which can be seen from the *spatial* Fourier transform of, e.g., $\delta(x-ct)$:

$$\int_{-\infty}^{\infty}\delta(x-ct)\,e^{-ikx}\,dx = e^{-ikct} = e^{-i\omega t},$$

with $\omega = kc$. For the different velocities, $\omega_1 = kc_1$, whereas $\omega_2 = kc_2$. Hence, $\omega_2 = (c_2/c_1)\,\omega_1$. Hence, if the propagation

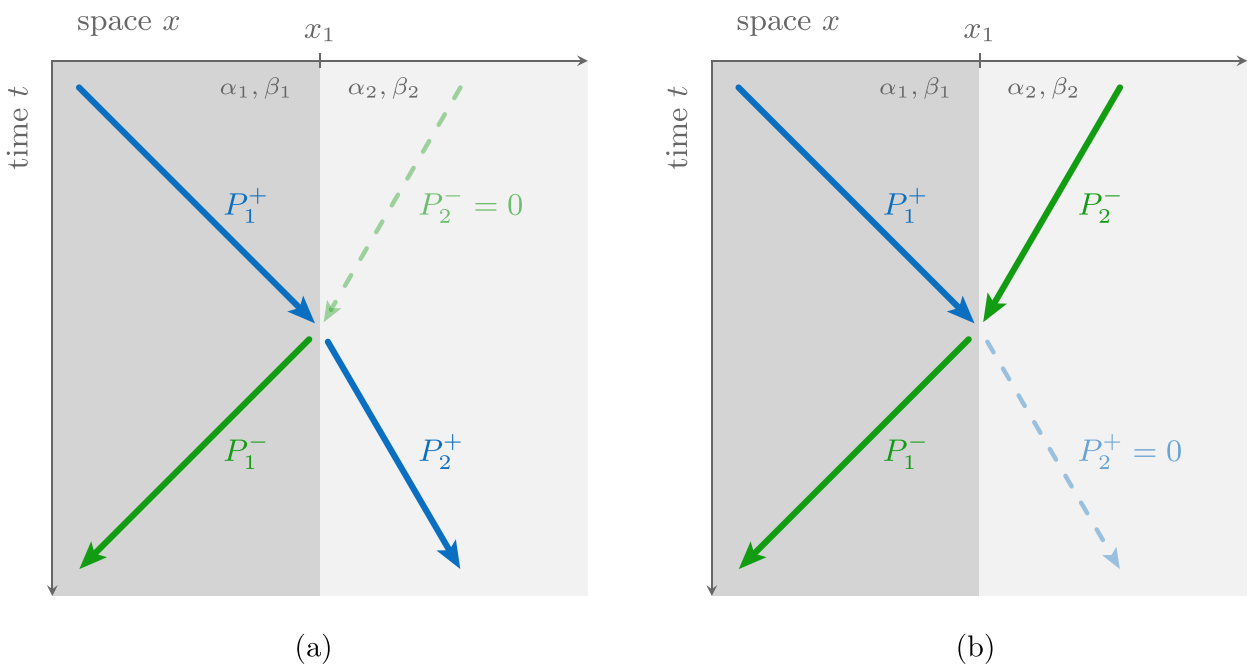

FIG. 1. Normal and special forward scattering at a space boundary at x_1 in the (x, t) plane. Ray slopes are inversely proportional to the propagation velocity and grays encode AC/TE impedances (SH/TM admittances). Right-going waves are blue, and left-going waves are green. (a) Normal forward scattering: A right-going wave is incident from the left and no left-going wave is present on the right. (b) Special forward scattering: Waves are incident from *both* sides with an amplitude and phase relation that cancels the right-going wave on the right.

velocity changes across the boundary, the scattered waves will experience a frequency shift proportional to the ratio of the propagation velocities [22].

C. Reverse-space transmission and reflection coefficients and relation with the time coefficients

We now analyze normal forward scattering at a spatial boundary in the a-causal direction (i.e., backward) and derive associated transmission and reflection coefficients, T^f and R^f. These are shown to be scaled versions of the time transmission and reflection coefficients.

As the starting point, we use again the system of equations derived for the space boundary, i.e., Eq. (8), but instead of dividing by the amplitude of the incident wave, we divide by the amplitude of the transmitted wave, to define reverse-space transmission and reflection coefficients: $T^f = A_I^x/A_T^x$ and $R^f = A_R^x/A_T^x$. Solving for T^f and R^f, we find

$$T_{12}^f = \left(\frac{\eta_2 + \eta_1}{2\eta_2}\right), \tag{16a}$$

$$R_{12}^f = \left(\frac{\eta_2 - \eta_1}{2\eta_2}\right), \tag{16b}$$

where the first digit in the subscripts of T^f and R^f refers to the medium with two phases present and $T_{12}^f = \{T_{21}^x\}^{-1}$.

Comparing Eq. (16) to Eq. (15), we see that, provided the indices are swapped, the reverse-space transmission and reflection coefficients are indeed scaled versions of the time transmission and reflection coefficients:

$$T_{21}^f = \left(\frac{c_1}{c_2}\right) T_{12}^t, \tag{17a}$$

$$R_{21}^f = -\left(\frac{c_1}{c_2}\right) R_{12}^t. \tag{17b}$$

Note that the scale factors for the transmission and reflection coefficients have the same magnitude, but not the same sign. Despite the opposing sign, this allows us to establish a partial (but useful) mapping later between wave fields produced by time scattering, and so-called focusing wave fields as introduced in the next section.

D. Focusing wave fields

Before explaining exactly what focusing wave fields are, and how we can construct them, it is useful to briefly contrast two different types of forward scattering in Fig. 1.

Figure 1, left, depicts *normal* forward scattering: A wave, P_1^+, incident on an interface from the left produces reflected and transmitted waves, P_1^- and P_2^+, respectively.

Figure 1, right, depicts *special* forward scattering: Waves incident both from the left (P_1^+) and from the right (P_2^-), when properly tuned, produce only scattered waves on the left (P_1^-).

Normally, both the incident wave from the left and the incident wave from the right produce scattered, right-going waves (P_2^+). The only way for these to cancel is if the transmitted wave from the left destructively interferes with the reflected wave from the right. That implies a very specific amplitude

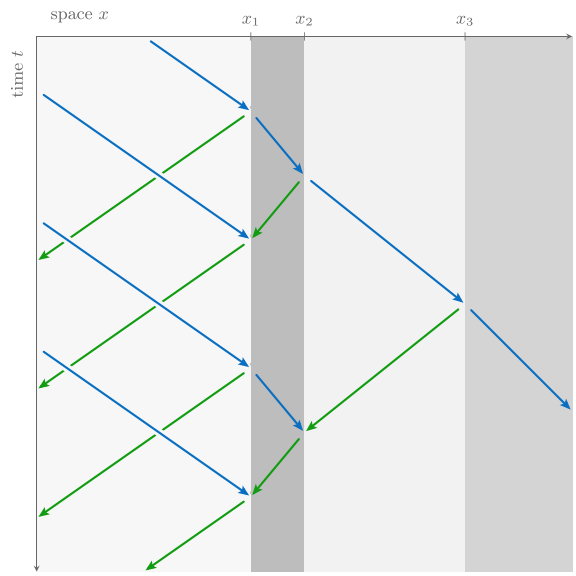

FIG. 2. A focusing wave field, built up recursively from the right, across space boundaries at x_3, x_2, and x_1, by repeatedly applying Eq. (16). Grays encode impedances (admittances) as in Fig. 1. The 2^{3-1} waves incident from the left are timed and scaled so that all rightward reflections of left-going waves cancel and a *single* right-going wave emerges beyond x_3.

(and phase) relation between the waves incident from the left and from the right.

In Appendix A, it is shown that Eq. (16) also governs the partitioning of amplitudes in the case of special forward scattering.

Recursive construction

The two cases of forward scattering shown in Fig. 1 can be combined recursively to construct a so-called focusing wave field (see Fig. 2). This wave field inherits the special property from Fig. 1, right, that left-going waves do not produce right-going reflections (and vice versa, when considering a mirrored configuration). As a result, focusing wave fields produce a single, transmitted wave when propagating through a stack of layers, effectively suppressing all internal reverberations.

So far, we have focused on amplitudes: Equation (16) governs the partitioning at each interface when recursively constructing the focusing wave field. However, from Fig. 1, right, it is clear that the incident waves must also arrive at the interface *simultaneously* in order to effect the special forward scattering. Nevertheless, it is straightforward to include the phase in the recursive construction.

For example, starting with a single, right-going wave, P^+_{j+1}, immediately right of an interface separating layers j and $j+1$, application of Eq. (16) yields the amplitudes of the right- and left-going waves P^+_j and P^-_j immediately to the left of that interface. These right- and left-going waves are then extrapolated further leftward, to the interface separating layers $j-1$ and j. This can be done by applying appropriate phase factors: Leftward extrapolation of a *right-going* wave amounts to propagating the wave *backward* in time and therefore should *remove* phase, whereas leftward extrapolation of a *left-going* wave amounts to propagating the wave *forward* in time and therefore should *add* phase. Equation (16) can then be applied again to each individual, leftward-extrapolated wave, yielding two pairs of right- and left-going waves (i.e., four events in total) to be extrapolated. The whole process is repeated, until the leftmost interface is crossed, to yield the complete focusing wave field (see Fig. 2).

E. Time scattering

Scattering at a time boundary is schematically illustrated in Fig. 3 for a left- and a right-going wave. The instant that the material properties change, the left- and right-going waves are partially reflected and transmitted with coefficients R^t and T^t, respectively.

By transposing the space and time axes of Fig. 3, one notices a similarity with Fig. 1, right: Due to causality, waves scattering at a time boundary cannot reflect into the past, just like we enforce "spatial causality" when constructing a focusing wave field recursively by evaluating Eq. (16) in one direction only. This explains the absence of upward-pointing arrows in Fig. 3 and of rightward reflections in Figs. 1 (right) and 2. Indeed, it has been noted that scattering at multiple time boundaries is simpler than scattering at multiple space boundaries because the infinite recursion due to waves reverberating between the space boundaries is avoided [24].

In Fig. 4, a wave scattering at multiple time boundaries is considered. At every time boundary, the wave front splits into two, thus doubling the number of events. This situation can be compared to Fig. 2, for the focusing wave field. In both figures, left-going waves are shown in green, while right-going waves are shown in dark blue. The similarities are striking, and one figure can be obtained from the other by transposing it [32]. Now, the reason for the suggestive naming in Eq. (16) is clear: In order to map the time scattering onto the focusing wave fields, the time transmission and reflection coefficients must have exactly the same *form*, up to a scale factor, as indeed we have shown in Eq. (17).

III. MEDIA THAT COMPUTE THEIR OWN INVERSE

The possibility of constructing a medium that computes its own inverse now becomes apparent when considering Fig. 4 in combination with Fig. 2. Placing Fig. 4 above and to the left of Fig. 2 suggests that a single wave scattering at a sequence of time boundaries could yield the focusing wave field that focuses through a sequence of space boundaries. Thus, a space-time medium can be nontrivially inhomogeneous in space *and* time and support complex forward scattering while still being able to collapse that scattering back onto a single pulse.

At first sight, it may seem that the minus sign appearing in Eq. (17) precludes a one-to-one mapping between the time-scattered wave fields and the focusing wave fields since it implies that time-reflected waves have the wrong sign compared to the required reverse-space reflection coefficient. However, since all the transmitted waves in the time-scattered wave field undergo an *even* number of time reflections, this is not the case. Furthermore, since the scaling in Eq. (17) does not affect the *ratio* of the time transmission and reflection coefficients, the transmitted part of the resulting

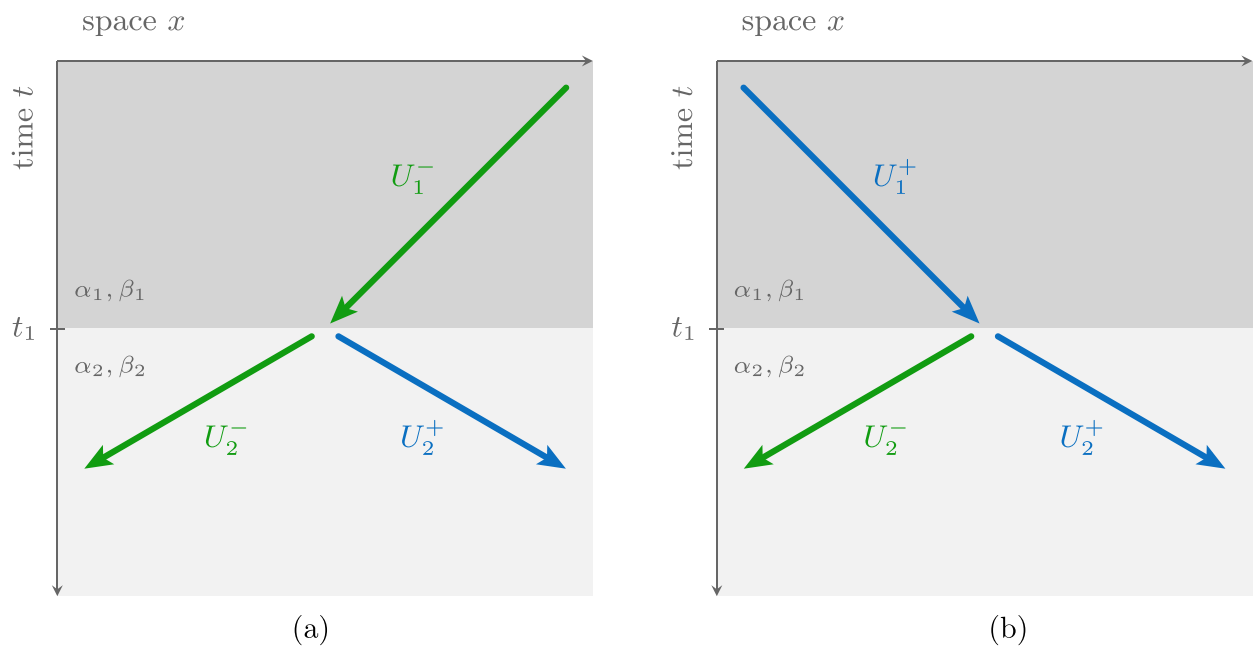

FIG. 3. Scattering at a single time boundary at t_1, with the same conventions as in Fig. 1. Due to causality, no waves scatter into the past. Because the material properties change at t_1, *both* scattered waves leave the boundary with a slope different from that of the incident wave—a signature of a time boundary. (a) Left-going and (b) right-going incident waves.

time-scattered wave field can still be mapped onto a focusing wave field.

To finalize the mapping, we only need to consider how a single space layer with thickness h_j^x and propagation velocity c_j maps onto a single time layer. In order to reproduce a particular one-way time delay or advance Δ_j^t, we need to translate this time delay to a one-way space delay or advance Δ_j^x, respectively. Considering a connecting layer of constant propagation velocity, c_c, we can define the Δ_j^x in terms of the Δ_j^t as $\Delta_j^x = c_c \Delta_j^t$. Hence, the time duration of the individual time layers can be found as

$$h_j^t = \Delta_j^x / c_j = c_c \Delta_j^t / c_j = c_c h_j^x / c_j^2. \tag{18}$$

Note that the time duration of the individual time layers, h_j^t, is indeed the only thing that needs to be computed since we have already established that the time reflection and transmission coefficients feature the same velocities and densities that occur in the reverse-space reflection and transmission coefficients. The time durations are a function of the propagation velocity of the connecting layer since the connecting layer is what allows mapping the time delays and advances in the focusing wave field onto the space delays and advances in the time scattering.

Finally, it should be mentioned that while any connecting layer propagation velocity and density will yield a valid focusing wave field that yields a single pulse on the other side of the spatial inhomogeneity, only a connecting layer propagation velocity and density equal to the propagation velocity and density of the first time (last spatial) will yield a transmission coefficient of unity since only then the product of the individual frequency shifts occurring at every time boundary is unity.

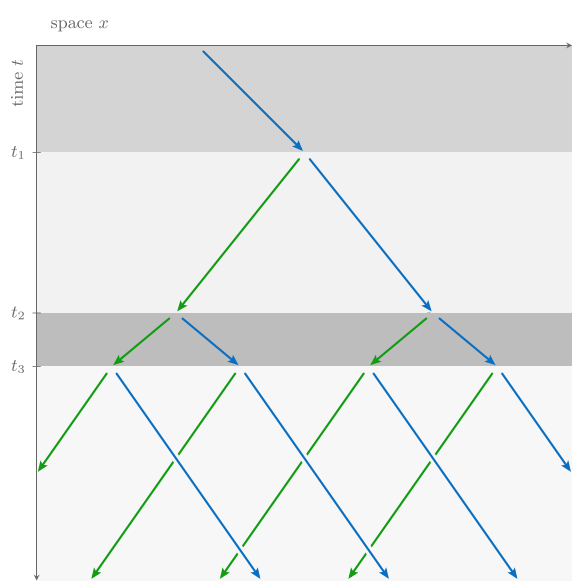

FIG. 4. A single wave scattering at time boundaries at t_1, t_2, and t_3, shown with the same conventions as Fig. 2. Comparing the figures, this is the exact transpose of Fig. 2, including the impedances (admittances), but with the direction of the blue arrows reversed. A single wave incident on a sequence of time boundaries therefore generates exactly the set of events that a layered medium needs as its focusing wave field.

IV. EXAMPLE

In Fig. 5, a numerical example of a space-time medium that computes its own inverse is shown. In the bottom right of the medium, a spatial inhomogeneity is located, consisting of three layers of varying thickness, propagation velocity, and density, embedded in a medium of higher propagation velocity (see Table II). Using Eq. (18) and a connecting layer propagation velocity $c_c = 1500$ m/s, the time durations of the

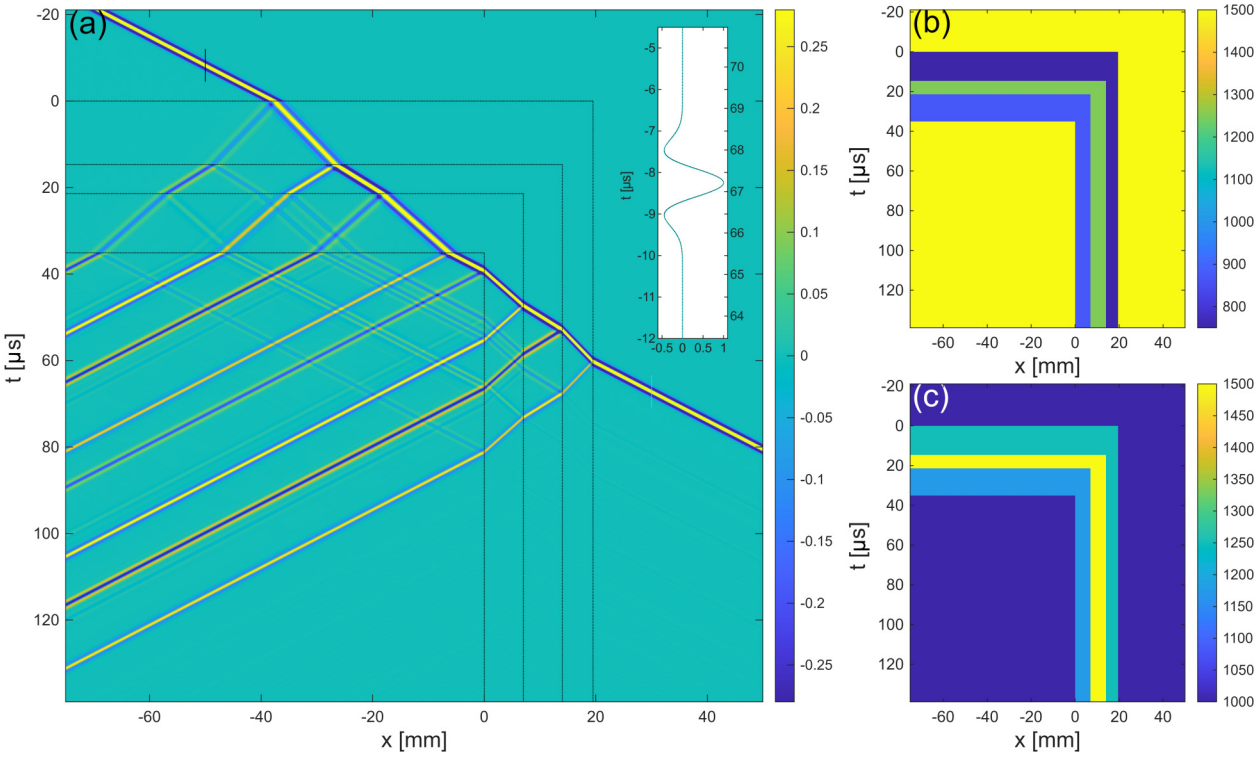

FIG. 5. Medium computing its own inverse. (a) Wave field with inset showing the incident and the transmitted wave. (b) Propagation velocity ($\mathrm{m\,s^{-1}}$). (c) Mass density ($\mathrm{kg\,m^{-3}}$). See text for details.

corresponding temporal inhomogeneities were computed. The resulting durations to be used in the top left of the simulation are also given in Table II.

To model the propagation in the space-time medium, a staggered-grid finite-difference time-domain algorithm with simple absorbing boundaries was used. The material property matrices (propagation velocity and density) used in the simulation are shown in Figs. 5(b) and 5(c), respectively. For every time step of the simulation, a corresponding row of these matrices is used. Between each time step, the P and Q fields are converted to U and V and back, to apply the temporal continuity conditions. The resulting wave field for an ultrasonic source on the left of the medium excited at early times with a Ricker wavelet (second derivative of a Gaussian) with center frequency $f_c = 500$ kHz is shown in Fig. 5(a).

As can be seen in Fig. 5(a), the single incident pulse first scatters into 2, then 4, then 8, and finally into 16 events upon encountering the four time boundaries (present after $t = 0$). Eight of these events are right-going and propagate toward the spatial inhomogeneities (present after $x = 0$). Upon interacting with the spatial inhomogeneity, we can see that the timing of these incident waves is such that rightward reflections of leftward reflections of the initial pulse are suppressed. Thus, only a single transmitted pulse is observed on the right of the spatial inhomogeneity, confirming that the field incident on the spatial inhomogeneity indeed consists of the focusing wave field. Furthermore, inspection of the single transmitted pulse confirms that it has the same wavelet and amplitude as the original incident pulse, such that we can say that the transmission coefficient of the inhomogeneous space-time medium is unity and therefore that the medium has computed its own inverse.

The full MATLAB code used to compute the example is included in Appendix B.

TABLE II. Space-time medium properties.

Layer	Thickness (mm)	Duration (μs)	Propagation velocity ($\mathrm{m\,s^{-1}}$)	Density ($\mathrm{kg\,m^{-3}}$)
1	∞	∞	1500	1000
2	7.0	13.71	875	1175
3	7.0	6.72	1250	1500
4	5.5	14.67	750	1250
5	∞	∞	1500	1000

V. DISCUSSION AND CONCLUSION

The existence of 1D acoustic, electromagnetic, and elastic space-time media that compute their own inverse has been demonstrated. Because the medium is time and space variant, basic properties such as linear time invariance and existence of an impulse response and the output being the convolution of an arbitrary input with such an impulse response are no longer guaranteed. However, we note that the construction of the medium does not rely on a fixed space-time "offset" of the time and space boundaries: Provided that the connecting layer is "large" enough (in time and space), an impulse response can be defined and longer inputs can be considered for which the output will still be the convolution with the impulse response. Conversely, note that even for a single incident pulse, there must be sufficient space available to accommodate

all the time scattering. In the example, both the extent of the domain and the timing of the first time boundary have been chosen such that the scattering at the last time boundary takes place before the leftmost left-going wave hits the left edge of the domain and the rightmost right-going wave hits the spatial discontinuity. Since it is only the relative spacing/timing of the incident waves that matters, provided that we are able to extend the background/embedding medium, it is always possible, at least in 1D, to create enough space-time between the time boundaries and the space boundaries such that a medium computing its own inverse can be constructed.

When the connecting layer has the same propagation velocity and density as the last spatial (first time) layer, the transmission coefficient of the system is unity. However, the left-reflected field is clearly nonzero, consisting of both left-going waves resulting from the time scattering and leftward reflections of the focusing wave field.

The possible applications of such a medium are many. One could think of environments where it is physically impossible to place hardware, but where the medium as a whole can be manipulated. In such a case, a single incoming pulse can be manipulated such that it anticipates certain undesired reverberations at spatial inhomogeneities. The most likely candidate for experimental realization is ultrasonics in fluids, where previous work has shown the ability of modifying the acoustic medium through electrorheological effects [33]. The physics community is just beginning to explore the possibilities of wave control using space-time boundaries.

ACKNOWLEDGMENT

This work received funding from SNF Grant No. 197182.

APPENDIX A: PROOF THAT THE REVERSE-SPACE COEFFICIENTS ALSO APPLY TO SPECIAL FORWARD SCATTERING

To prove that Eq. (16) also applies to special forward scattering, we must show (with reference to Fig. 1, right)

(1) on the right: that the transmitted wave from the left destructively interferes with the reflected wave from the right, and

(2) on the left: that the superposition of the reflected wave from the left and the transmitted wave from the right equal the reverse-space transmission coefficient.

Taking $P_2^- = 1$, Eq. (16) predicts that $P_1^+ = R_{12}^f$ and $P_1^- = T_{12}^f$. Hence, the first condition can be written as

$$T_{12}^x R_{12}^f + R_{21}^x = 0. \tag{A1}$$

Submitting the relevant expressions [Eqs. (9a), (16b), and (9b)] into Eq. (A1), while paying attention to swapped indices, we find for the left-hand side:

$$\left(\frac{2\eta_2}{\eta_2+\eta_1}\right)\left(\frac{\eta_2-\eta_1}{2\eta_2}\right)+\left(\frac{\eta_1-\eta_2}{\eta_1+\eta_2}\right),$$

which is indeed zero, so that condition (1) [Eq. (A1)] is satisfied. The second condition yields

$$R_{12}^x R_{12}^f + T_{21}^x = T_{12}^f. \tag{A2}$$

Again, submitting the relevant expressions [Eqs. (9b), (16b), and (9a)] into Eq. (A2), we find

$$\left(\frac{\eta_2-\eta_1}{\eta_2+\eta_1}\right)\left(\frac{\eta_2-\eta_1}{2\eta_2}\right)+\left(\frac{2\eta_1}{\eta_1+\eta_2}\right) = \frac{\eta_1^2+\eta_2^2-2\eta_1\eta_2}{2\eta_2(\eta_2+\eta_1)}+\frac{4\eta_1\eta_2}{2\eta_2(\eta_2+\eta_1)} = \frac{(\eta_2+\eta_1)^2}{2\eta_2(\eta_2+\eta_1)},$$

which does indeed equate to T_{12}^f [cf. Eq. (16a)] so that condition (2) [Eq. (A2)] is also satisfied.

APPENDIX B: MATLAB CODE FOR THE EXAMPLE

```
% Acoustic example
b0=1000; c0=1500; % background density [kg/m^3] and sound speed [m/s]
bs_x=[1175,1500,1250]; % mass densities [kg/m^3]
cs_x=[875,1250,750]; % sound speeds [m/s]
xs_x=[7,7,5.5]/1000; % space layer thicknesses [m]
dx=0.0125/1000; fc=500*1000; kc=fc/c0; % space step [m], central frequency [Hz]
[bm,cm,dt,itsrc,xsrc]=disc_med(b0,c0,bs_x,cs_x,xs_x,dx,fc); % discretize medium
[P_all,Q_all,ts_out,xs_out]=fdtd(bm,cm,dt,dx,kc,itsrc,xsrc); % compute scattering
figure; imagesc(xs_out,ts_out,P_all); clim(clim/2.5); xlabel('x[m]'); ylabel('t[s]');

function [bm,cm,dt,itinj,xsrc]=disc_med(b0,c0,bs_x,cs_x,xs_x,dx,fc)
    dt=0.99*dx/max([c0 cs_x]); nx_buff=500;
    xsrc=2*c0/fc; ixsrc=floor(xsrc/dx)+1; itinj=20; itsrc=floor(2/(fc*dt))+1;
    % compute time variations for spatial variations, space for time scattering
    ts_t=fliplr(c0*xs_x./cs_x.^2); cs_t=fliplr(cs_x); bs_t=fliplr(bs_x);
    xs_t_tot=sum(cs_t.*ts_t); xs_x_tot=sum(xs_x);
    % compute position of spatial and temporal variations, medium size and init
    ix0=ixsrc+floor(2*xs_t_tot/dx)+1+nx_buff; it0=itinj+floor(xs_t_tot/(c0*dt))+1;
    nt=it0+floor(sum(ts_t)/dt)+floor((2*xs_t_tot+nx_buff*dx)/(c0*dt))+itsrc+1;
```

```
    nx=ix0+floor(xs_x_tot/dx)+ixsrc+1; bm=b0*ones(nt,nx); cm=c0*ones(nt,nx);
    % build actual time-space corner model
    its=cumsum([it0 round(ts_t/dt)]); ixs=cumsum([ix0 round(xs_x/dx)]);
    for ii=1:length(cs_x)
        bm(its(ii):its(ii+1),1:ixs(end-ii)-1)=bs_t(ii);
        cm(its(ii):its(ii+1),1:ixs(end-ii)-1)=cs_t(ii);
        bm(its(end-ii):end,ixs(ii):ixs(ii+1))=bs_x(ii);
        cm(its(end-ii):end,ixs(ii):ixs(ii+1))=cs_x(ii);
    end
end

function [P_all,Q_all,ts,xs]=fdtd(bm,cm,dt,dx,kc,it,xsrc)
    [nt,nx]=size(cm); ts=dt*(0:nt-1); xs=dx*(0:nx-1);
    % extend medium on left and right to avoid boundary reflections
    nx_left=nx; nx_right=nx; nx_e=nx_left+nx+nx_right;
    bm_e=[repmat(bm(:,1),1,nx_left) bm repmat(bm(:,nx),1,nx_right)];
    cm_e=[repmat(cm(:,1),1,nx_left) cm repmat(cm(:,nx),1,nx_right)];
    xs_e=[xs(1)-dx*(nx_left:-1:1) xs xs(nx)+dx*(1:nx_right)];
    % initialize arrays, computational constants and spatial wavelet
    P_all=zeros(nt,nx); P=zeros(1,nx_e);
    Q_all=zeros(nt,nx); Q=zeros(1,nx_e);
    c1m=dt.*bm_e.*cm_e.^2; c2m=dt./bm_e;
    qsrc=(1-2*pi^2*kc^2*(xs_e-xsrc).^2).*exp(-(pi*kc*(xs_e-xsrc)).^2);
    % main fdtd loop with U and V continuous between time steps
    for ii=2:nt
        P(1,:)=P(1,:).*(bm_e(ii,:).*cm_e(ii,:).^2)./(bm_e(ii-1,:).*cm_e(ii-1,:).^2);
        Q(1,1:end-1)=Q(1,1:end-1)-c2m(ii,1:end-1).*diff(P,1,2)/dx;
        if ii==it, Q(1,:)=Q(1,:)+qsrc./(bm_e(ii,:).*cm_e(ii,:)); end
        Q(1,:)=Q(1,:).*bm_e(ii-1,:)./bm_e(ii,:);
        P(1,2:end)=P(1,2:end)-c1m(ii,2:end).*diff(Q,1,2)/dx;
        if ii==it, P(1,:)=P(1,:)+qsrc; end
        P_all(ii,:)=P(1,nx_left+(1:nx));
        Q_all(ii,:)=Q(1,nx_left+(1:nx));
    end
end
```


[1] D. Horsman, S. Stepney, R. C. Wagner, and V. Kendon, When does a physical system compute? Proc. R. Soc. A **470**, 20140182 (2014).

[2] H. Jaeger, B. Noheda, and W. G. van der Wiel, Toward a formal theory for computing machines made out of whatever physics offers, Nat. Commun. **14**, 4911 (2023).

[3] G. Tanaka, T. Yamane, J. B. Héroux, R. Nakane, N. Kanazawa, S. Takeda, H. Numata, D. Nakano, and A. Hirose, Recent advances in physical reservoir computing: A review, Neural Networks **115**, 100 (2019).

[4] T. Inagaki, Y. Haribara, K. Igarashi, T. Sonobe, S. Tamate, T. Honjo, A. Marandi, P. L. McMahon, T. Umeki, K. Enbutsu, *et al.*, A coherent Ising machine for 2000-node optimization problems, Science **354**, 603 (2016).

[5] I. Oguz, N. Dinc, M. Yildirim, J. Ke, I. Yoo, Q. Wang, F. Yang, C. Moser, and D. Psaltis, Optical diffusion models for image generation, Adv. Neural Inf. Process. Syst. **37**, 59150 (2024).

[6] A. Cordaro, B. Edwards, V. Nikkhah, A. Alù, N. Engheta, and A. Polman, Solving integral equations in free space with inverse-designed ultrathin optical metagratings, Nat. Nanotechnol. **18**, 365 (2023).

[7] F. Zangeneh-Nejad, D. L. Sounas, A. Alù, and R. Fleury, Analogue computing with metamaterials, Nat. Rev. Mater. **6**, 207 (2021).

[8] T. W. Hughes, I. A. Williamson, M. Minkov, and S. Fan, Wave physics as an analog recurrent neural network, Sci. Adv. **5**, eaay6946 (2019).

[9] T. Dubček, D. Moreno-Garcia, T. Haag, P. Omidvar, H. R. Thomsen, T. S. Becker, L. Gebraad, C. Bärlocher, F. Andersson, S. D. Huber, *et al.*, In-sensor passive speech classification with phononic metamaterials, Adv. Funct. Mater. **34**, 2311877 (2024).

[10] J. Weng, Y. Ding, C. Hu, X.-F. Zhu, B. Liang, J. Yang, and J. Cheng, Meta-neural-network for real-time and passive deep-learning-based object recognition, Nat. Commun. **11**, 6309 (2020).

[11] C. Qian, Z. Wang, H. Qian, T. Cai, B. Zheng, X. Lin, Y. Shen, I. Kaminer, E. Li, and H. Chen, Dynamic recognition

and mirage using neuro-metamaterials, Nat. Commun. **13**, 2694 (2022).

[12] A. Fichtner, H.-P. Bunge, and H. Igel, The adjoint method in seismology: I. Theory, Phys. Earth Planet. Interact. **157**, 86 (2006).

[13] J. Tromp, C. Tape, and Q. Liu, Seismic tomography, adjoint methods, time reversal and banana-doughnut kernels, Geophys. J. Int. **160**, 195 (2005).

[14] P. J. Werbos, Backpropagation through time: What it does and how to do it, Proc. IEEE **78**, 1550 (1990).

[15] R. J. Williams and D. Zipser, A learning algorithm for continually running fully recurrent neural networks, Neural Comput. **1**, 270 (1989).

[16] M. Hermans, B. Schrauwen, P. Bienstman, and J. Dambre, Automated design of complex dynamic systems, PLoS One **9**, e86696 (2014).

[17] V. Lopez-Pastor and F. Marquardt, Self-learning machines based on Hamiltonian echo backpropagation, Phys. Rev. X **13**, 031020 (2023).

[18] G. Pourcel and M. Ernoult, Learning long range dependencies through time reversal symmetry breaking, Adv. Neural Info. Proc. Syst. **38**, 72615 (2026).

[19] G. Pourcel, D. Basu, M. Ernoult, and A. Gilra, Lagrangian-based equilibrium propagation: Generalisation to arbitrary boundary conditions & equivalence with Hamiltonian echo learning, arXiv:2506.06248.

[20] N. D. Cin, F. Marquardt, and C. C. Wanjura, Training nonlinear optical neural networks with scattering backpropagation, arXiv:2508.11750.

[21] F. Morgenthaler, Velocity modulation of electromagnetic waves, IRE Trans. Microwave Theory Tech. **6**, 167 (1958).

[22] J. T. Mendonça and P. K. Shukla, Time refraction and time reflection: Two basic concepts, Phys. Scr. **65**, 160 (2002).

[23] V. Bacot, M. Labousse, A. Eddi, M. Fink, and E. Fort, Time reversal and holography with spacetime transformations, Nat. Phys. **12**, 972 (2016).

[24] M. A. Salem and C. Caloz, Space-time cross-mapping and application to wave scattering, arXiv:1504.02012.

[25] K. Wapenaar, F. Broggini, E. Slob, and R. Snieder, Three-dimensional single-sided Marchenko inverse scattering, data-driven focusing, Green's function retrieval, and their mutual relations, Phys. Rev. Lett. **110**, 084301 (2013).

[26] K. Wapenaar, J. Thorbecke, J. van der Neut, F. Broggini, E. Slob, and R. Snieder, Marchenko imaging, Geophysics **79**, WA39 (2014).

[27] T. T. Koutserimpas and R. Fleury, Electromagnetic fields in a time-varying medium: Exceptional points and operator symmetries, IEEE Trans. Antennas Propag. **68**, 6717 (2020).

[28] K. Wapenaar, Green's functions, propagation invariants, reciprocity theorems, wave-field representations, and propagator matrices in two-dimensional time-dependent materials, Proc. R. Soc. A **481**, 20240479 (2025).

[29] K. Wapenaar and E. C. Slob, Green's matrix and propagator matrix for three-dimensional electromagnetic wave propagation and scattering in a time-variant material, Prog. Electromagn. Res. **186**, 11 (2026).

[30] K. Wapenaar, J. Aichele, and D.-J. van Manen, Waves in space-dependent and time-dependent materials: A systematic comparison, Wave Motion **130**, 103374 (2024).

[31] C. Caloz and Z. L. Deck-Léger, Spacetime metamaterials—Part II: Theory and applications, IEEE Trans. Antennas Propag. **68**, 1583 (2020).

[32] Note that even if the time-scattered and focusing wave fields can be mapped onto each other bijectively, the arrows are not all pointing in the same direction. Therefore, one must be cautious when interpreting this mapping and the corresponding physics.

[33] L. Li, M. Wang, J. Wang, and X. Zhao, The control of ultrasonic transmission by the metamaterials structure of electrorheological fluid and metal foam, Smart Mater. Struct. **26**, 115006 (2017).